J. Phys. F: Met. Phys. **18** (1988) 469–483. Printed in the UK

Density functional theory of non-collinear magnetism

J Kübler†, K-H Höck†, J Sticht† and A R Williams‡

† Institut für Festkörperphysik, Technische Hochschule Darmstadt, D-6100 Darmstadt, FRG

‡ IBM Thomas J Watson Research Center, Yorktown Heights, NY 10598, USA

Received 28 May 1987

Abstract. We formulate a density functional theory (DF) to describe non-collinear magnetism. Self-consistent, spin-polarised energy-band calculations based on the local approximation to DF theory are presented in which the magnetisation associated with different atoms in a unit cell is allowed to point along different, non-collinear directions. Non-self-consistent calculations employing non-collinear quantisation axes have been presented before; the present calculations are, we believe, distinguished by: first, being self-consistent; second, providing the total energy; and third, providing the spin-quantisation axes. In our first applications we deal with the non-collinear antiferromagnets γ-FeMn, $RhMn_3$, and $PtMn_3$ and show that their total energies are minimised in the tetrahedral (FeMn) or triangular ($RhMn_3$, $PtMn_3$) magnetic structures first proposed by Kouvel and Kasper.

1. Introduction

Numerous spin-density functional calculations of the energy band structure and related electronic properties of ferromagnetic and antiferromagnetic materials have appeared in the recent literature. Koelling (1981) has compiled a listing of papers on band structure calculations which also contains work on magnetic systems and covers the field up to about 1980. Since then some 50 more papers on this subject were published—far too many to deal with here. Yet, a small selection must be made to illustrate the field. Thus very recent and representative examples are the work by Wang *et al* (1985) and Moruzzi *et al* (1986) on magnetic and structural ordering in Fe, Co and Ni. Binary intermetallics and compounds were studied among many others by Malozemoff *et al* (1984) and Coehoorn *et al* (1985). Work on ternary compounds is reviewed by one of the authors (Kübler 1984) and by de Groot and Buschow (1986) and a discussion of transition-metal oxides can be found in a paper by Kübler and Williams (1986).

Common to all of these theories and calculations is the treatment of the magnetic moment as having only two directions, namely up and down, as in the Ising model. We call these moment arrangements collinear.

It was first in work on disordered magnetic moments in the CPA approximation (Oguchi *et al* 1983, Pindor *et al* 1983) and in models using spin spirals (You and Heine 1982, Haines *et al* 1985) that the magnetic moment was treated as a vector observable

0305-4608/88/030469 + 15 $02.50

and non-collinear arrangements were admitted. Non-collinear order was also considered by Cade (1981) in an attempt to understand the antiferromagnetism of Mn and, very recently, Sandratskii and Guletskii (1986) obtained the non-self-consistent band-structure of a spin spiral in Fe and deduced the energy of a 'frozen' spin wave.

Starting from density functional theory (Kohn and Sham 1965, von Barth and Hedin 1972) we here derive the effective single-particle equations for non-collinear magnets; i.e. in the crystalline systems which we have in mind the spin-quantisation axis is allowed to vary from site to site. However, we shall see that the orientation of the axes with respect to some frame of reference is not arbitrary; rather it is a property of the ground state and thus, in contrast to other work on non-collinear magnets, it is an output quantity. Although the theory predicts well defined sets of directions for the spins, it does not couple the latter to the underlying crystal lattice, all that is important is their relative orientation. This changes when spin–orbit coupling (SOC) is added to the Hamiltonian. Except perhaps for the lanthanides and actinides, a typical energy implied by SOC is an order of magnitude smaller than the spin–spin interaction energies in non-collinear arrangements; still, SOC effectively supplies the coupling of the magnetic moments to the crystal lattice thus giving rise to anisotropy. Hence, this theory is a prerequisite to calculations of magnetic anisotropy (Sticht 1988).

Using the local approximation to density functional theory, the effective single-particle equations can be solved self-consistently and the total energy thereby obtained. The latter is used to single out the correct ground state in those cases where more than one set of spin-quantisation axes is possible. We implement the theory using the ASW method (Williams *et al* 1979) and apply it to calculations of non-collinear antiferromagnets which are characterised by an order parameter having a wave vector $\boldsymbol{q}=0$; examples of these are 'tetrahedral' (γ-FeMn) and 'triangular' ($RhMn_3$ and $PtMn_3$) antiferromagnetic systems (Endoh and Ishikawa 1971, Kouvel and Kasper 1965, Krén *et al* 1967).

2. Formulation of the problem

Following von Barth and Hedin (1972) we write down density functional theory using as an external potential the 2×2 matrix with elements $w_{\alpha\beta}(\boldsymbol{r})$. Let the elements of the density matrix be $\rho_{\alpha\beta}(\boldsymbol{r})$. The electron density is then $\operatorname{Tr}\boldsymbol{\rho}\doteq n(\boldsymbol{r})$ and the total energy becomes

$$E\{\rho_{\alpha\beta}\}=T_0+\sum_{\alpha\beta}\int w_{\alpha\beta}(\boldsymbol{r})\rho_{\beta\alpha}(\boldsymbol{r})\,\mathrm{d}^3r+\int\int\frac{n(\boldsymbol{r}')n(\boldsymbol{r})}{|\boldsymbol{r}-\boldsymbol{r}'|}\,\mathrm{d}^3r\,\mathrm{d}^3r'+E_{\mathrm{xc}}\{\rho_{\alpha\beta}\}. \tag{1}$$

T_0 is the kinetic energy of non-interacting electrons, and E_{xc} is the exchange-correlation energy. The variational properties of $E\{\rho_{\alpha\beta}\}$ were proved exhaustively by von Barth and Hedin (1972) and, therefore, need not be discussed here any further. Next the effective single-particle equation is written as

$$\sum_{\beta}\left(-\delta_{\alpha\beta}\nabla^2+w_{\alpha\beta}^{\mathrm{eff}}(\boldsymbol{r})\right)\varphi_{\beta i}(\boldsymbol{r})=\varepsilon_i\varphi_{\alpha i}(\boldsymbol{r}) \tag{2}$$

whence the kinetic energy, T_0, is obtained

$$T_0 = \sum_{i \in \text{occ}} \varepsilon_i - \sum_{\alpha\beta} \int w^{\text{eff}}_{\alpha\beta}(\boldsymbol{r}) \rho_{\beta\alpha}(\boldsymbol{r})\, \mathrm{d}^3 r \tag{3}$$

where occ stands for the lowest occupied states, the $\varphi_{\alpha i}$ are assumed to be normalised, and the single-particle density matrix is

$$\rho_{\alpha\beta}(\boldsymbol{r}) = \sum_{i \in \text{occ}} \varphi_{\alpha i}(\boldsymbol{r}) \varphi^*_{\beta i}(\boldsymbol{r}). \tag{4}$$

If we substitute equation (3) into equation (1), we obtain the total energy E as a functional of $\rho_{\alpha\beta}$ and can determine $w^{\text{eff}}_{\alpha\beta}$ by using the variational properties of $E\{\rho_{\alpha\beta}\}$. One easily obtains

$$w^{\text{eff}}_{\beta\alpha}(\boldsymbol{r}) = w_{\beta\alpha}(\boldsymbol{r}) + 2\delta_{\alpha\beta} \int \frac{n(\boldsymbol{r}')}{|\boldsymbol{r} - \boldsymbol{r}'|}\, \mathrm{d}^3 r' + \frac{\delta E_{\text{xc}}\{\rho_{\alpha\beta}\}}{\delta \rho_{\alpha\beta}}. \tag{5}$$

Now, $E_{\text{xc}}\{\rho_{\alpha\beta}\}$ is not known in general. But we know it for a gas of interacting electrons which can be spin polarised. This means for the homogeneous case we know E_{xc} as a function of the eigenvalues of the density matrix, ρ_1 and ρ_2,

$$E_{\text{xc}} = E_{\text{xc}}\{\rho_1, \rho_2\} = \int n(\boldsymbol{r}) \varepsilon_{\text{xc}}(\rho_1(\boldsymbol{r}), \rho_2(\boldsymbol{r}))\, \mathrm{d}^3 r, \tag{6}$$

where $n(\boldsymbol{r})$ is the trace, $n(\boldsymbol{r}) = \rho_1(\boldsymbol{r}) + \rho_2(\boldsymbol{r})$. In the local approximation to density functional theory we admit inhomogeneous densities ρ_1 and ρ_2 and use equation (6) to approximate E_{xc}. In this case, the density matrix is given by equation (4) and is not necessarily diagonal, but we may assume there is a unitary transformation, $\mathbf{U}$, which diagonalises it locally, i.e., for $i = 1, 2$

$$\sum_{\alpha\beta} U_{i\alpha} \rho_{\alpha\beta} U^+_{\beta i} = \rho_i \tag{7}$$

implying an $\boldsymbol{r}$ dependence in all quantities.

Using equation (7) and for $\mathbf{U}$ the well known spin-$\frac{1}{2}$ rotation matrix,

$$\mathbf{U} = \begin{pmatrix} \exp(\frac{1}{2}\mathrm{i}\varphi_\nu) \cos\frac{1}{2}\theta_\nu & \exp(-\frac{1}{2}\mathrm{i}\varphi_\nu) \sin\frac{1}{2}\theta_\nu \\ -\exp(\frac{1}{2}\mathrm{i}\varphi_\nu) \sin\frac{1}{2}\theta_\nu & \exp(-\frac{1}{2}\mathrm{i}\varphi_\nu) \cos\frac{1}{2}\theta_\nu \end{pmatrix}$$

we express $\partial E_{\text{xc}}/\partial \rho_{\alpha\beta}$ in terms of $\partial E_{\text{xc}}/\partial \rho_i$ and the angles θ_ν, φ_ν, and obtain from equation (5) the effective single-particle 'potential matrix'

$$\mathbf{w}^{\text{eff}}(\boldsymbol{r}) = v_0(\boldsymbol{r})\mathbf{1} + \Delta v(\boldsymbol{r})\tilde{\boldsymbol{\sigma}}_z. \tag{8}$$

Here $\tilde{\boldsymbol{\sigma}}_z$ is the z component of the Pauli spin matrix in a coordinate system which is rotated by the polar angles θ_ν, φ_ν with respect to a fixed coordinate system,

$$\tilde{\boldsymbol{\sigma}}_z = \begin{pmatrix} \cos\theta_\nu & \exp(-\mathrm{i}\varphi_\nu)\sin\theta_\nu \\ \exp(\mathrm{i}\varphi_\nu)\sin\theta_\nu & -\cos\theta_\nu \end{pmatrix} \tag{9}$$

1 is the unit 2×2 matrix, the quantity $v_0(\boldsymbol{r})$ is given by

$$v_0(\boldsymbol{r}) = v(\boldsymbol{r}) + 2\int \frac{n(\boldsymbol{r}')}{|\boldsymbol{r}-\boldsymbol{r}'|}\,\mathrm{d}^3\boldsymbol{r}' + \tfrac{1}{2}(v_{\mathrm{xc1}}(\boldsymbol{r}) + v_{\mathrm{xc2}}(\boldsymbol{r})), \tag{10}$$

where $v(\boldsymbol{r})$ is the external potential, furthermore

$$v_{\mathrm{xci}}(\boldsymbol{r}) = \frac{\delta E_{\mathrm{xc}}}{\delta \rho_i} = \varepsilon_{\mathrm{xc}}(\rho_1, \rho_2) + n\frac{\partial \varepsilon_{\mathrm{xc}}}{\partial \rho_i} \qquad i = 1, 2 \tag{11}$$

and

$$\Delta v(\boldsymbol{r}) = \tfrac{1}{2}(v_{\mathrm{xc1}}(\boldsymbol{r}) - v_{\mathrm{xc2}}(\boldsymbol{r})). \tag{12}$$

The derivation so far in principle implies angles θ_ν and φ_ν that are $\boldsymbol{r}$ dependent because of the local diagonalisation, equation (7). An essential simplification is achieved by the atomic sphere approximation (ASA) and the requirement that at each point within a given sphere the spin-quantisation axis is the same, but different spheres may have different axes. This way we basically exchange a fine-grained mesh for a coarse-grained one. The index ν then labels a site defined by the νth atomic sphere (AS) and the angles θ_ν, φ_ν are obtained by diagonalising the integrated density matrix; i.e. we define for each site the 'charge'

$$q_{\alpha\beta}^{(\nu)} = \int_{S_\nu} \rho_{\alpha\beta}(\boldsymbol{r})\,\mathrm{d}^3 r \tag{13}$$

where S_ν labels the νth AS, then

$$\sum_{\alpha\beta} U_{i\alpha}^{(\nu)} q_{\alpha\beta}^{(\nu)} U_{\beta j}^{(\nu)+} = q_i^{(\nu)}\delta_{ij} \tag{14}$$

is diagonal as indicated provided the angles are

$$\theta_\nu = \tan^{-1}\frac{2\Delta_\nu}{a_\nu - d_\nu}$$

and (15)

$$\varphi_\nu = -\tan^{-1}\frac{\mathrm{Im}\{b_\nu\}}{\mathrm{Re}\{b_\nu\}},$$

where

$$a_\nu = q_{11}^{(\nu)}$$

$$b_\nu = q_{12}^{(\nu)}$$

$$d_\nu = q_{22}^{(\nu)}$$

and

$$\Delta_\nu = \mathrm{Re}\{b_\nu\}\cos\varphi_\nu - \mathrm{Im}\{b_\nu\}\sin\varphi_\nu.$$

The matrix $\mathbf{U}^{(\nu)}$ is then used in equation (7) to obtain the eigenvalues $\rho_1(\boldsymbol{r})$ and $\rho_2(\boldsymbol{r})$ of the density matrix in each atomic sphere.

This completes the specificaton of the effective single-particle equations for non-collinear magnetic systems (collinear systems obviously are just a special case) and the physics is very much like that described by You and Heine (1982). The electron travelling through the crystal experiences exchange-correlation forces that vary from site to site. These polarise the electron system resulting, in general, in a non-diagonal density and 'charge' matrix. Its diagonalisation *defines* quantisation axes locally (i.e. for each atomic sphere) and hence a local direction of magnetisation. As normal with density functional theory the calculation needs to be made self-consistent, a requirement which besides charge and magnitude of the local magnetisation now applies also to the directions of the local magnetic moments. However, as You and Heine (1982) pointed out, there may be occasions when strict self-consistency is not desirable, as for instance in functional–integral theories where the local spin-quantisation axes are treated as parameters.

We close this section by giving a convenient expression for the total energy for those cases where the calculation is self-consistent. It is easily verified that, starting with equations (1) and (3), the total energy can be written as

$$E=\sum_{i\in\mathrm{occ}}\varepsilon_i-\int\int\frac{n(\boldsymbol{r})n(\boldsymbol{r}')}{|\boldsymbol{r}-\boldsymbol{r}'|}\,\mathrm{d}^3r\,\mathrm{d}^3r'-\tfrac{1}{2}\int n^2\left(\frac{\partial\varepsilon_{\mathrm{xc}}}{\partial\rho_1}+\frac{\partial\varepsilon_{\mathrm{xc}}}{\partial\rho_2}\right)\mathrm{d}^3r-\sum_{\alpha\beta}\int\Delta v_{\alpha\beta}\rho_{\beta\alpha}\,\mathrm{d}^3r, \qquad (16)$$

where $\Delta v_{\alpha\beta}=\frac{1}{2}(v_{\mathrm{xc}1}-v_{\mathrm{xc}2})\tilde{\sigma}_{z,\alpha\beta}$, see equations (9) and (12). We may use the transformation given by equation (7) to eliminate $\rho_{\beta\alpha}$ from equation (16) even in cases where the quantity $\mathbf{U}^{(\nu)}\boldsymbol{\rho}\mathbf{U}^{(\nu)\dagger}$ is not strictly diagonal.

The result is

$$E=\sum_{i\in\mathrm{occ}}\varepsilon_i-\int\int\frac{n(\boldsymbol{r})n(\boldsymbol{r}')}{|\boldsymbol{r}-\boldsymbol{r}'|}\,\mathrm{d}^3r\,\mathrm{d}^3r'-\sum_{\alpha}\int\mathrm{d}^3r n(\boldsymbol{r})\frac{\partial\varepsilon_{\mathrm{xc}}}{\partial\rho_\alpha}\rho_\alpha(\boldsymbol{r}) \qquad (17)$$

where we used that at self-consistency (where input angles are equal to output angles) we have

$$\mathbf{U}^{(\nu)}\tilde{\boldsymbol{\sigma}}_z\mathbf{U}^{(\nu)\dagger}=\begin{pmatrix}1 & 0\\ 0 & -1\end{pmatrix}.$$

One sees that the total energy is entirely expressed in terms of the density, n, the diagonal elements of the transformed density matrix, ρ_α, and the single-particle energies, ε_i. Thus it is as easy to evaluate as for the usual collinear cases.

3. Implementation

The effective single-particle equation (2) can be solved numerically without great effort if one is willing to use a linearised scheme together with the atomic sphere approximation; examples are the LMTO method (Andersen 1975) or the ASW method (Williams *et al* 1979, henceforth referred to as WKG). We use the latter and begin by

defining the basis functions. These are chosen to be made up of numerical solutions of the Schrödinger equation,

$$(-\nabla^2 + v_0(\boldsymbol{r}) - \varepsilon_{l\nu}^{(X)})\chi_{L\nu}^{(X)}(\boldsymbol{r}) = 0. \tag{18}$$

The notation is such that the index ν implies $\boldsymbol{r}$ to lie in the atomic sphere (AS) ν; L denotes both the angular momentum and the magnetic quantum number, $L = (l, m)$, and $v_0(\boldsymbol{r})$ is the spin-independent part of the effective potential as given by equation (10). It is constructed to be spherically symmetric in each AS. The radial parts of $\chi_{L\nu}^{(X)}$ are required to satisfy Hankel function boundary conditions, $X = H$, and those of $\chi_{L\nu}^{(X=J)}$ Bessel function boundary conditions (see WKG) at $r = S_\nu$, where S_ν is the radius of the AS ν. The basis functions can now be specified; at $\boldsymbol{r}$ within the AS ν centred at $\boldsymbol{\tau}_\nu$ in the unit cell they are

$$\varphi_{\alpha k}(\boldsymbol{r}) = \sum_{L\mu} C_{\alpha L\mu}(k)\left(\chi_{L\nu}^{(H)}(\boldsymbol{r})\delta_{\nu,\mu} + \sum_{L'} \chi_{L'\nu}^{(J)}(\boldsymbol{r}) B_{L'L}(\boldsymbol{\tau}_\nu - \boldsymbol{\tau}_\mu, \boldsymbol{k})\right). \tag{19}$$

The coefficients $C_{\alpha L\mu}(k)$, $\alpha = 1, 2$, are obtained from a variational treatment of equation (2); $\boldsymbol{k}$ is a vector in the Brillouin zone and k implies both $\boldsymbol{k}$ and the band index. The quantities $B_{L'L}(\boldsymbol{\tau}_\nu - \boldsymbol{\tau}_\mu, \boldsymbol{k})$ are the KKR structure constants for a system with basis vectors $\{\boldsymbol{\tau}_\nu\}$. The first term in the brackets on the right-hand side of equation (19) represents augmented Hankel functions centred at the AS ν in which $\boldsymbol{r}$ lies and the second represents the augmented tails of all Hankel functions centred at AS other than ν.

Next, the overlap and Hamiltonian matrices, $\mathbf{S}$ and $\mathcal{H}$, are set up. With the spinor notation,

$$\psi_k(\boldsymbol{r}) = \begin{pmatrix} \varphi_{1k}(\boldsymbol{r}) \\ \varphi_{2k}(\boldsymbol{r}) \end{pmatrix}$$

where the right-hand side is defined by equation (19), the overlap matrix, $\mathbf{S}$, is easily seen to be block diagonal with two identical blocks which are exactly the ones of the standard ASW treatment of WKG. The Hamiltonian matrix can be written as a sum of a block diagonal one, $\overline{\mathcal{H}}_0$, plus $\overline{\mathcal{H}}_1$. $\overline{\mathcal{H}}_0$ consists, like $\mathbf{S}$, of two identical parts, which have exactly the form of the usual ASW Hamiltonian matrix, $\overline{\mathcal{H}}_{\mathrm{ASW}}$, see equation (29) of WKG,

$$\overline{\mathcal{H}}_0 = \begin{pmatrix} \overline{\mathcal{H}}_{\mathrm{ASW}} & 0 \\ 0 & \overline{\mathcal{H}}_{\mathrm{ASW}} \end{pmatrix}.$$

$\overline{\mathcal{H}}_1$ alone comprises the spin-dependent part of the problem. It consists of the matrix elements

$$\langle \sigma \nu L | \mathcal{H}_1 | L' \nu' \sigma' \rangle$$

using equations (8) and (9) and suppressing the wave-vector index, $\boldsymbol{k}$, we find for the diagonal blocks

$$\begin{aligned}\langle 1\nu L|\mathcal{H}_1|L'\nu' 1\rangle &= -\langle 2\nu L|\mathcal{H}_1|L'\nu' 2\rangle \\ &= \delta_{LL'}\delta_{\nu\nu'}\cos\theta_\nu f^{H,H}_{L\nu} + B^{+}_{LL'}(\boldsymbol{\tau}_\nu - \boldsymbol{\tau}_{\nu'}, \boldsymbol{k})\cos\theta_{\nu'} f^{H,J}_{L'\nu'} \\ &\quad + \cos\theta_\nu f^{H,J}_{L\nu} B_{LL'}(\boldsymbol{\tau}_\nu - \boldsymbol{\tau}_{\nu'}, \boldsymbol{k}) \\ &\quad + \sum_{\nu''}\sum_{L''} B^{+}_{LL''}(\boldsymbol{\tau}_\nu - \boldsymbol{\tau}_{\nu''}, \boldsymbol{k})\cos\theta_{\nu''} f^{J,J}_{L''\nu''} B_{L''L'}(\boldsymbol{\tau}_{\nu''} - \boldsymbol{\tau}_{\nu'}, \boldsymbol{k})\end{aligned} \tag{22}$$

where

$$f^{X,Y}_{L\nu} = \int_{S_\nu} r^2\,\mathrm{d}r\, R^{(X)}_{l\nu}(r)\Delta v(r) R^{(Y)}_{l\nu}(r) \tag{23}$$

with $X = H$ or J, $R^{(X)}_{l\nu}$ being the radial parts of $\chi^{(X)}_{L\nu}$ discussed at the beginning of this paragraph, and $\Delta v(r)$ given by equation (12).

The off-diagonal block is $\langle 1\nu L|\mathcal{H}_1|L'\nu' 2\rangle$. It follows from the right-hand side of equation (22) by replacing $\cos\theta_\nu$ by $\exp(-\mathrm{i}\varphi_\nu)\sin\theta_\nu$. Having defined $\overline{\mathcal{H}}$ and $\mathbf{S}$, we numerically diagonalise

$$\overline{\mathcal{H}} - \varepsilon\mathbf{S}$$

which gives the desired eigenvalues ε and eigenvectors

$$\mathbf{C} = \begin{pmatrix} C_{1L\nu} \\ C_{2L\nu} \end{pmatrix}. \tag{24}$$

These quantities enable us to construct partial state densities, $N_{l\nu\alpha\beta}(\varepsilon)$, and from these charge and spin densities. Generalising the procedure of WKG slightly we write

$$N_{l\nu\alpha\beta}(\varepsilon) = \sum_k \delta(\varepsilon - \varepsilon(k)) q_{l\nu\alpha\beta}(k) \tag{25}$$

where k implies wave vector and band index, and $q_{l\nu\alpha\beta}(k)$, for equal spin indices, $\alpha = \beta$, is the decomposed single-electron norm for angular momentum l and site ν. In all cases, spin diagonal or not, $q_{l\nu\alpha\beta}(k)$ is obtained from

$$\begin{aligned}q_{l\nu\alpha\beta}(k) = \sum_{m=-l}^{l} &(C^{*}_{\beta L\nu}(k)\langle HL\nu|HL\nu\rangle C_{\alpha L\nu}(k) + C^{*}_{\beta L\nu}(k)\langle HL\nu|JL\nu\rangle A_{\alpha L\nu}(k) \\ &+ A^{*}_{\beta L\nu}(k)\langle JL\nu|HL\nu\rangle C_{\alpha L\nu}(k) + A^{*}_{\beta L\nu}(k)\langle JL\nu|JL\nu\rangle A_{\alpha L\nu}(k))\end{aligned} \tag{26}$$

where

$$A_{\alpha L\nu}(k) = \sum_{L'\mu} B_{LL'}(\boldsymbol{\tau}_\nu - \boldsymbol{\tau}_\mu, \boldsymbol{k}) C_{\alpha L'\mu}(k)$$

and the vectors appearing in the matrix elements are those implied by equation (18).

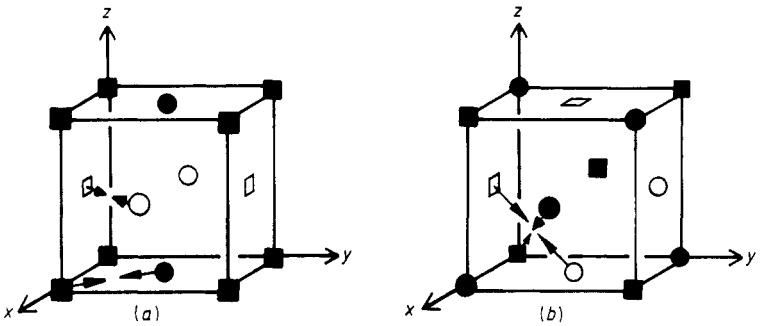

Figure 1. (*a*) Magnet unit cell of γ-FeMn having simple cubic primitive translations. Arrows shown define a non-collinear moment arrangement. (*b*) An alternative possible arrangement for γ-FeMn. Primitive translations here are (1, 0, 1), (1, 1, 0) and $(0, \frac{1}{2}, \frac{1}{2})$ in terms of the axes shown. The magnetic unit cell is trigonal. Fe: ■, 'right'; ●, 'left'. Mn: □, 'right'; ○, 'left'.

Now, the 'charge' defined by equation (13) is obtained by integrating the state density up to the Fermi energy ε_F:

$$q_{\alpha\beta}^{(\nu)} = \sum_l \int^{\epsilon_F} N_{l\nu\alpha\beta}(\varepsilon)\, d\varepsilon \tag{27}$$

and the matrices $\mathbf{U}^{(\nu)}$ are those which diagonalise $q_{\alpha\beta}^{(\nu)}$ for each site ν. The density-of-states matrix $N_{l\nu\alpha\beta}(\varepsilon)$ is subsequently transformed by means of $\mathbf{U}^{(\nu)}$

$$\sum_{\alpha\beta} U_{i\alpha}^{(\nu)} N_{l\nu\alpha\beta}(\varepsilon) U_{\beta i}^{(\nu)+} = N_{l\nu i}(\varepsilon) \tag{28}$$

for $i = 1, 2$. The quantity $N_{l\nu i}(\varepsilon)$ represents the state density in the local (atomic) frame of reference for spin up, $i = 1$, and spin down, $i = 2$. Finally, the moment analysis described by WKG is carried out for $N_{l\nu i}(\varepsilon)$ which yields the local-frame charge density $\rho_i(\boldsymbol{r})$, $i = 1, 2$, for each site.

4. Results

4.1. Antiferromagnetic γ-FeMn

Experimentally antiferromagnetic γ-FeMn alloys have been investigated extensively in the past, two important references being Kouvel and Kasper (1963) and Endoh and Ishikawa (1971). For the first time, we can now examine critically the magnetic order that was proposed for these alloys. Restricting ourselves to the ordered FeMn compound in the one-to-one stoichiometry (which may be fictitious since real FeMn alloys always seem to be disordered), we consider the two crystal structures depicted in figure 1. In the case of figure 1(*a*) the primitive translations are simple cubic, in the case of figure 1(*b*) these are the vectors (1, 0, 1), (1, 1, 0), and $(0, \frac{1}{2}, \frac{1}{2})$ in terms of the axes shown. Open symbols stand for Mn, closed ones for Fe, and circular and square symbols denote different spin directions. If, in the case of figure 1(*a*), 'right' and 'left' are strictly taken to be parallel to the y-axis—which is not the case drawn—then the

magnetic order is antiferromagnetic collinear (AF–COL); the order implied by the figure 1(*a*) with arrows pointing at each other as shown is obviously antiferromagnetic non-collinear (AF–N–COL). The same applies to figure 1(*b*) which also admits an obvious collinear and non-collinear antiferromagnetic order.

Our calculations were carried out for these four different cases: (i) collinear, (ii) non-collinear based on figure 1(*a*); (iii) collinear and (iv) non-collinear based on figure 1(*b*). For the lattice constant we used $a = 3.60$ Å, which we estimated from the thermal expansion coefficients given by Stamm (1987) to be the one appropriate at $T = 0$ K. Attempts to calculate the equilibrium volume were begun but discontinued after it became clear that the calculated volumes tended to be much too small. We see the reason for this in a local-density functional error which is largest in the case of Mn; this can already be seen in the results of Moruzzi *et al* (1978, p 6). Note that there the agreement between the measured and calculated quantities is good except for the cases with a half-filled shell, in particular manganese. This will not change when Mn is calculated including its magnetism. Our calculated magnetic moments, in the local (atomic) frame of reference, and the total energies, referred to the total energy of calculation (ii) are collected in table 1, which also contains an estimate of an experimental value for the average magnetic moment. The non-collinear magnetic order depicted in figure 1(*a*) has the lowest total energy and it can also be inferred from the work of Endoh and Ishikawa (1971) to be the probable ground-state order. But the antiferromagnetic collinear order (i) is seen to be only 13.5 meV higher in energy, corresponding to approximately 40 K per atom. (The Néel temperature is $T_N = 470$ K (Endoh and Ishikawa 1971).) The other magnetic moment arrangements (calculations (iii) and (iv)) can be excluded in view of their high total energies. All arrangements were self-consistent, however.

We now turn to the energy-band structure of the two cases having the lowest total energy. In a first step it is convenient to simplify matters by omitting the exchange splitting. Thus figure 2 shows the band structure obtained with a self-consistent potential, but setting $\Delta v = 0$ (equation (8)) in the calculation of the single-particle energies. Although it is clear from figure 1(*a*) that the symmetry is lower than cubic, the band structure is, nevertheless, easily understood in terms of the one of an FCC transition metal folding its Brillouin zone into that of the simple cubic lattice. Referring, therefore, to the well known band structure of Cu, e.g., we identify in figure 2 the bottom of the band as the Γ_1 s state, the nearly threefold degenerate state (marked 1 + 2) below the Fermi energy, ε_F, as the $\Gamma_{25'}$ d state and the two states just above ε_F as the Γ_{12} state. The two states in between Γ_1 and $\Gamma_{25'}$ are nearly threefold

Table 1. Calculated magnetic moments for antiferromagnetic γ-FeMn. m_{Fe}, m_{Mn}, magnetic moments of Fe and Mn, respectively, in multiples of μ_B; $\bar{m}$, average moment; E_{tot}, total energy per unit cell referred to total energy of calculation (ii); $\bar{m}_{exp}$ is an estimated experimental $T = 0$ K average magnetic moment (Endoh and Ishikawa 1971).

Magnetic order	m_{Fe}	m_{Mn}	$\bar{m}$	E_{tot} (meV)	$\bar{m}_{exp}$
(i) AF–COL (figure 1(*a*))	1.21	2.05	1.63	13.5	
(ii) AF–N–COL (figure 1(*a*))	1.41	2.09	1.75	0	~1.5
(iii) AF–COL (figure 1(*b*))	0.91	1.44	1.18	248.0	
(iv) AF–N–COL (figure 1(*b*))	0.73	1.32	1.03	249.0	

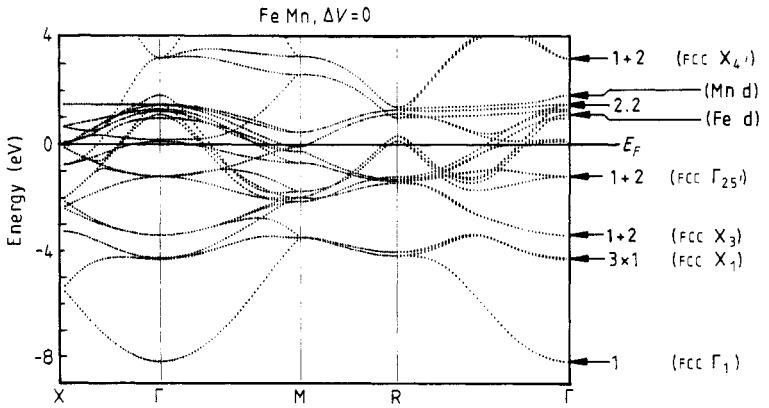

Figure 2. Band structure of γ-FeMn with exchange splitting set zero. The band labels on the right margin are those of an FCC transition metal. k-point labels X, Γ, M, R appropriate for SC Brillouin zone.

degenerate each and originate from X_3 and X_1, respectively. Above ε_F there are two non-degenerate states whose wavefunctions are either pure Fe d or pure Mn d (so marked); these states originate from one member of the X_5 state which is commonly taken as the top of the d band. The remaining states at Γ in figure 2 originate from X_2, the other member of X_5 (the fourfold degenerate state marked 2, 2) and from $X_{4'}$, the latter having p symmetry.

The band structure of hypothetical non-magnetic FeMn now helps enormously to clarify the real band structure. Figure 3 applies to antiferromagnetic collinear γ-FeMn, (*a*) showing the local, spin-up and spin-down, d-state density of Fe, (*c*) that for Mn and (*b*) giving the band structure. Figure 4 similarly applies to the antiferromagnetic non-collinear structure, the state densities shown here are defined by equation (28) and thus the arrows ↑ and ↓ refer to the atomic, local frames of reference which have the orientations of the arrows in figure 1(*a*). Figures 3 and 4, on first sight, are quite similar. The state densities (DOS) are not rigidly shifted DOS as in ferromagnetic

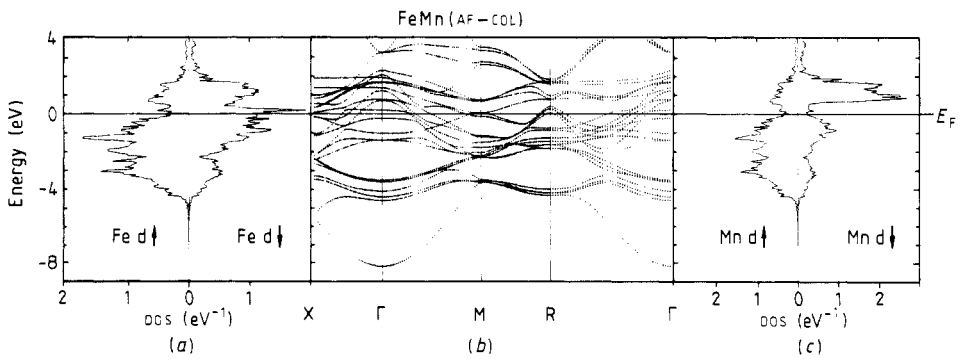

Figure 3. γ-FeMn, antiferromagnetic collinear based on unit cell shown in figure 1(*a*). (*a*) Partial density of states (DOS) of spin-up (↑) and spin-down (↓) Fe d electrons (per atom). (*b*) Band structure using same k-point labels as in figure 2. (*c*) Partial DOS of spin-up (↑) and spin-down (↓) Mn d electrons (per atom).

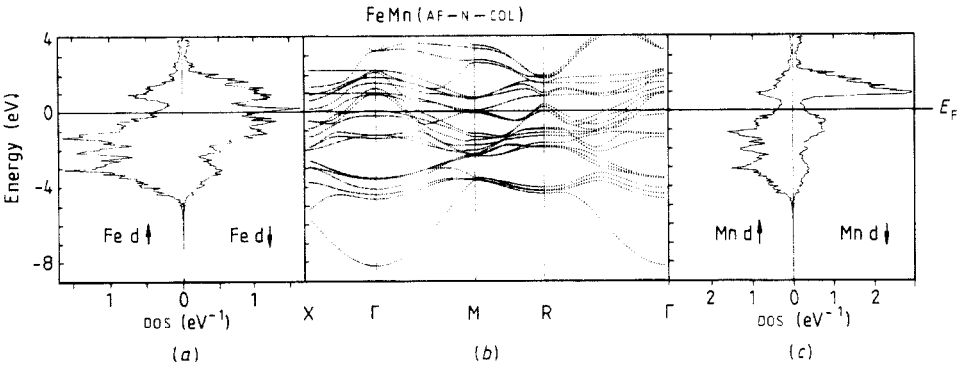

Figure 4. γ-FeMn non-collinear structure, orientation of local frames of references as shown by arrows in figure 1(*a*) ('tetrahedral'). (*a*) Partial DOS of spin-up (↑) and spin-down (↓) Fe d electrons (per atom) in the local frame of reference. (*b*) Band structure using same *k*-point labels as in figure 2. (*c*) Partial DOS of spin-up (↑) and spin-down (↓) Mn d electrons (per atom) in the local frame of reference.

metals, but are best described by shifted spectral weight and the notion of covalency (Williams *et al* 1981, 1982). Most features of the band structures, figure 3(*b*) and figure 4(*b*), are easily traced back to the appropriate states shown in figure 2 where degeneracies are lifted and states shifted. The amounts by which states are split or shifted are obviously different for the two magnetic structures. This is, e.g. quite pronounced for the very flat band 1.5 eV above ε_F in figure 2 at $X-\Gamma$ which is split by ~ 0.5 eV in figure 3(*b*), but 1.2 eV in figure 4(*b*). It is interesting to note that in the case of FCC Fe it is precisely this flat band that, if occupied, is believed to give rise to its high-spin state (Bagayoko and Callaway 1983). Furthermore, a gap is quite pronounced at ε_F half-way between X and Γ in figure 4(*b*), but is not present in the case of figure 3(*b*). It is not clear, however, if these different features can be identified experimentally.

4.2. *Antiferromagnetic $RhMn_3$*

From the experimental work of Kouvel and Kasper (1965) as well as Krén *et al* (1967) it is known that $RhMn_3$ has the Cu_3Au structure and orders antiferromagnetically with a Néel temperature of $T_N = 855$ K in a structure that is sometimes called 'triangular' and is shown in figure 5(*b*). Bertaut and Fruchart (1972) analysed group theoretically the transformation properties of this magnetic moment arrangement, calling it T_1 and describing another one, T_2, depicted in figure 5(*a*). Other antiferromagnetic moment arrangements are shown in figure 5(*c*), which is obviously collinear, and in figure 5(*d*) which is non-collinear. The four cases shown were investigated and found to be self-consistent moment arrangements. Again we had to use an experimental lattice constant instead of the calculated one (see § 4.1) and estimated from the published data (Krén *et al* 1967) $a = 3.8$ Å to be appropriate for $T = 0$ K. Our calculated magnetic moments in the local frame of reference and the total energies, referred to the total energy of the T_1 state are collected in table 2 which also contains an estimate of the experimental Mn moment. The total energy is lowest for T_1 or T_2, both structures giving identical results. This is not a failure of the theory but must, indeed,

be so. The reason for this is that our theory does not couple the magnetic moments to the underlying crystal lattice, all that is important is the relative orientation of the moments, and in this respect, T_1 and T_2 can be seen to be equal. Bertaut and Fruchart (1972) discussed the same facts when they pointed out that in the Heisenberg model T_1 and T_2 are identical as long as anisotropy is not included. This changes when spin–orbit coupling (SOC) is considered, i.e. SOC effectively supplies a coupling of the magnetic moments to the crystal structure thus giving rise to anisotropy.

We investigated numerically the changes of the total energy which are brought about by SOC. To do this one first goes over to using a different wave equation: the Schrödinger equation, equation (12), is replaced by the scalar-relativistic approximation to the Dirac equation (Koelling and Harmon 1977). Next one can show that the effective single-particle potential $\mathbf{w}^{\text{eff}}$, equation (8), contains an additional term, $\mathbf{v}_{\text{LS}}$, which describes SOC and has the form given by MacDonald *et al* (1980). The quantity $\mathbf{v}_{\text{LS}}$ is not spin diagonal and is, therefore, added to $\mathcal{H}_1$ (§3); this way both the exchange splitting, $\Delta\mathbf{v}$ and SOC are treated on the same footing, i.e. in particular, both terms are effective in the formation of the self-consistent single-particle potential. Full details will be published elsewhere (Sticht 1988). Numerically it was found that spin–orbit coupling favours the T_1 state by the small but definitive amount of 1.5 meV per unit cell.

The energy-band structure of the T_1 or T_2 states is, as before, most conveniently studied by first omitting the exchange splitting. The role of relativistic effects and SOC will not be considered at all here. Figure 6 shows the band-structure of hypothetical non-magnetic ($\Delta v \equiv 0$) $RhMn_3$.

Since $RhMn_3$ without magnetic order (in contrast to γ-FeMn) is cubic its band structure is unambiguously described by a folded, FCC transition-metal band structure, e.g. that of Cu. In figure 6 we therefore indicate the origin of the various states at Γ by again using the state labels of Cu. All states at Γ, except for the bottom of the band, which is non-degenerate, are at least threefold degenerate, not counting spin.

The antiferromagnetic order T_1 (or T_2) now breaks the symmetry resulting in a band structure with split and shifted states as depicted in figure 7(*b*). Figure 7(*a*) shows the local state densities (DOS) of the d states of Rh, and figure 7(*c*) those of Mn. As before, the DOS are defined by equation (28), therefore, the arrows $\uparrow$ and $\downarrow$ refer to the atomic, local frames of reference which have the orientations of the arrows in either figure 5(*a*) or (*b*). Although figure 7(*b*) is quite involved, one can,

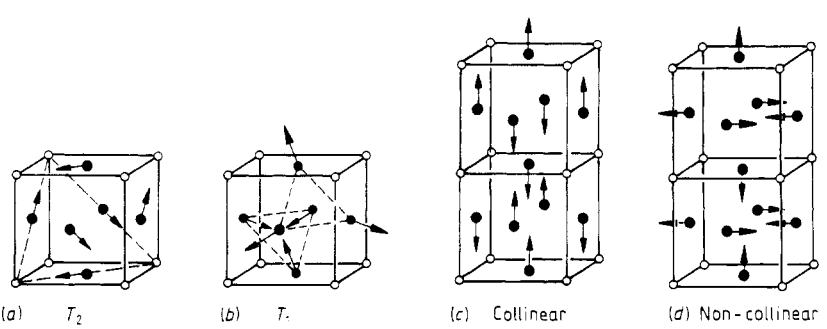

Figure 5. Possible magnetic moment arrangements for the Cu_3Au structure. (*a*) and (*b*) are 'triangular' or non-collinear, based on the chemical unit cell. (*c*) and (*d*) are based on the doubled cell.

Table 2. Calculated magnetic moments for antiferromagnetic $RhMn_3$. m_{Mn}, m_{Rh}, magnetic moments of Mn and Rh, respectively, in multiples of μ_B; E_{tot}, total energy per unit cell referred to total energy of (b) T_1. $m_{Mn,exp}$ is an estimated $T = 0$ K experimental magnetic moment (Krén *et al* 1967).

Magnetic order	m_{Mn}	m_{Rh}	E_{tot} (meV)	$m_{Mn,exp}$
(a) T_2	3.10	0	0	
(b) T_1	3.10	0	0	3.6 ± 0.4
(c) Collinear	3.05†	0.1	449	
(d) Non-collinear	3.02†	0.07	231	

† Average values.

nevertheless, determine the origin of most states by comparison with figure 6. One detail deserves mentioning and this is the splitting of the flat band which was discussed for FeMn in § 4.1. It is seen in figure 6 at 1.2 eV above ε_F for k vectors between X and Γ and gives rise to more than two bands in figure 7(*b*), one set being below ε_F. Comparing with figure 4(*b*) we recognise that this set of bands provides the additional states for the local up-direction that increase the manganese moment from $\sim 2\mu_B$ in γ-FeMn to $\sim 3\mu_B$ in $RhMn_3$. This is, indeed, similar to the high-spin state in FCC Fe (Bagayoko and Callaway 1983).

4.3. *Antiferromagnetic $PtMn_3$*

We close this section of applications by a brief discussion of the interesting system $PtMn_3$. Krén *et al* (1967, 1968) investigated an entire series of alloys of composition $Pt_{1-x}Rh_xMn_3$ and Krén *et al* (1971) presented an interesting phase diagram. According to this, at low temperatures the magnetic structure is triangular, but a first-order transition to a collinear state occurs at 365 K, the Néel temperature being $T_N = 475$ K and the magnetic moment of manganese $m_{Mn} = (3.0 \pm 0.3)\ \mu_B$ at low temperatures.

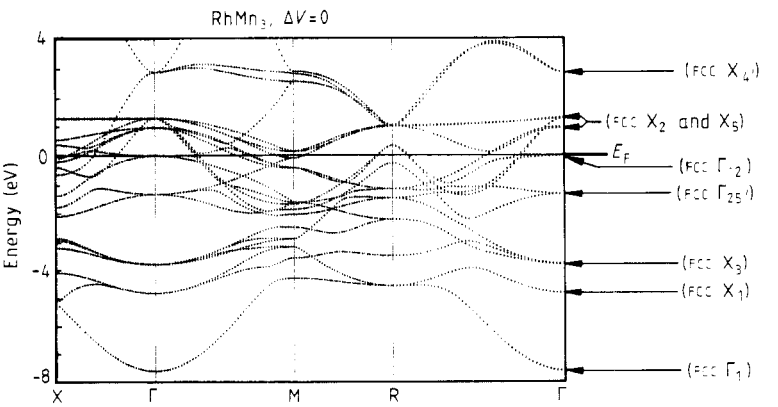

Figure 6. Band structure of $RhMn_3$ with exchange splitting set zero. The band labels on the right margin are those of an FCC transition metal. k-point labels X, Γ, M, R appropriate for SC Brillouin zone.

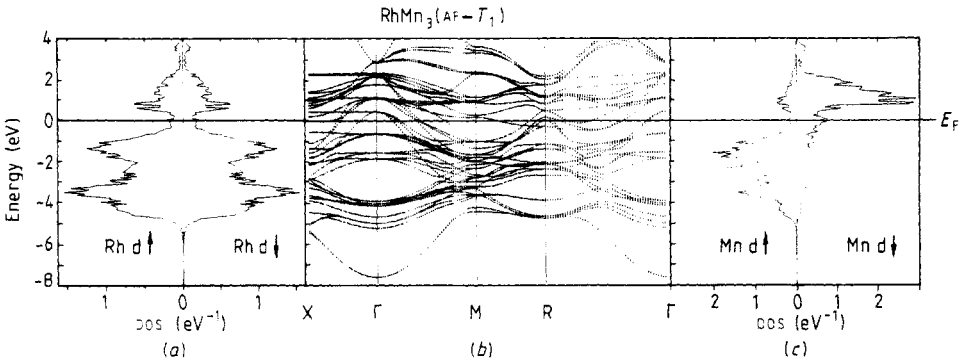

Figure 7. $RhMn_3$ non-collinear structure; orientation of local frames of reference either as shown by arrows in figure 5(*a*) (T_2) or figure 5(*b*) (T_1). (*a*) Partial DOS of spin-up (↑) and spin-down (↓) Rh d electrons, orientation of axis is arbitrary since moment is zero. (*b*) Band structure using same *k*-point labels as in figure 6. (*c*) Partial DOS of spin-up (↑) and spin-down (↓) Mn d electrons (per atom) in the local frame of reference.

With an estimated $T = 0$ K lattice constant of $a = 3.8$ Å we carried out calculations for assumed ferromagnetic $PtMn_3$ and two further sets of calculations for the different moment arrangements shown in figure 5. We discard the ferromagnetic ground state because its total energy is more than 1 eV higher than the antiferromagnetic ones. For the two sets of calculations with antiferromagnetic ground states we used the scalar relativistic equations, in the first neglecting spin–orbit coupling (SOC), in the second, however, considering SOC as described in § 4.2. The calculated magnetic moments did not depend on SOC, at least not within the precision shown in table 3, which summarises our results. Column 3 gives the total energy without, column 4 with SOC. Both types of calculations predict either T_1 or T_2 (no SOC) or T_1 (with SOC) to be the correct ground state, which is more stable than T_2 by 6 meV per cell. We may discard the collinear order shown in figure 5(*c*) because of its high total energy, but the non-collinear order with a doubled unit cell shown in figure 5(*d*) is only 123 meV per cell, or the equivalent of about 475 K per magnetic atom, higher than the ground state T_1. The magnetic order proposed by Krén *et al* (1971) does have a doubled unit cell but is collinear with zero-magnetic moments for some Mn atoms. We have not been able to 'prepare' such a magnetic moment arrangement.

Table 3. Calculated magnetic moments for antiferromagnetic $PtMn_3$. m_{Mn}, m_{Pt}, magnetic moments of Mn and Pt, respectively, in multiples of μ_B. Column 3: E_{tot}, total energy per unit cell referred to the total energy of (b) T_1 in the scalar relativistic approximation, but without SOC. Column 4: E_{tot} as column 3, but SOC included.

Magnetic order	m_{Mn}	m_{Pt}	E_{tot} (meV)	E_{tot} (meV)
(a) T_2	2.93	0	0	−265
(b) T_1	2.93	0	0	−271
(c) Collinear	2.99	0.08	432	—
(d) Non-collinear	2.93†	0.05	167	−148

† Average value.

Acknowledgment

We thank P Kelly for drawing our attention to some of the references dealing with non-collinear magnetism. Work was partially supported by SFB 252 Darmstadt/Frankfurt/Mainz.

References

Andersen O K 1975 *Phys. Rev.* B **12** 3060–83
Bagayoko D and Callaway J 1983 *Phys. Rev.* B **28** 5419–22
von Barth U and Hedin L 1972 *J. Phys. C: Solid State Phys.* **5** 1629–42
Bertaut F F and Fruchart D 1972 *Int. J. Magn.* **2** 259–64
Cade N A 1981 *Physics of Transition Metals 1980* ed. P Rhodes (Institute of Physics Conf. Series 55) pp 351–4
Coehoorn R, Haas C and de Groot R A 1985 *Phys. Rev.* B **31** 1980–6
de Groot R A and Buschow K H J 1986 *J. Magn. Magn. Mater.* **54–57** 1377–80
Endoh Y and Ishikawa Y 1971 *J. Phys. Soc. Japan* **30** 1614–27
Haines E M, Heine V and Ziegler A 1985 *J. Phys. F: Met. Phys.* **15** 661–74
Koelling D D 1981 *Rep. Prog. Phys.* **44** 144–212
Koelling D D and Harmon B N 1977 *J. Phys. C: Solid State Phys.* **10** 3107–14
Kohn W and Sham L J 1965 *Phys. Rev.* **140** A1133–8
Kouvel J S and Kasper J S 1963 *J. Phys. Chem. Sol.* **24** 529–36
—— 1965 *Proc. Int. Conf. on Magnetism, Nottingham 1964* (London: Institute of Physics and Physical Chemistry) pp 169–70
Krén E, Kádár G, Pál L and Szabó P 1967 *J. Appl. Phys.* **38** 1265–6
Krén E, Kádár G, Pál L, Sólyom J, Szabó P and Tarnoczi T 1968 *Phys. Rev.* **171** 574–85
Krén E, Zsoldas É, Barberon M and Fruchart R 1971 *Solid State Commun.* **9** 27–31
Kübler J 1984 *Physica* **127B** 257–63
Kübler J and Williams A R 1986 *J. Magn. Magn. Mater.* **54–57** 603–6
MacDonald A H, Pickett W F and Koelling D D 1980 *J. Phys. C: Solid State Phys.* **13** 2675–83
Malozemoff A P, Williams A R and Moruzzi V L 1984 *Phys. Rev.* B **29** 1620–32
Moruzzi V L, Williams A R and Janak J F 1978 *Calculated Electronic Properties of Metals* (New York: Pergamon)
Moruzzi V L, Marcus P M, Schwarz K and Mohn P 1986 *Phys. Rev.* B **34** 1784–91
Oguchi T, Terakura K and Hamada N 1983 *J. Phys. F: Met. Phys.* **13** 145–60
Pindor A J, Staunton J, Stocks G M and Winter H 1983 *J. Phys. F: Met. Phys.* **13** 979–89
Sandratskii L M and Guletskii P G 1986 *J. Phys. F: Met. Phys.* **16** L43–8
Stamm W 1987 private communication
Sticht J 1988 to be published
Wang C S, Klein B M and Krakauer H 1985 *Phys. Rev. Lett.* **54** 1852–5
Williams A R, Kübler J and Gelatt C D Jr 1979 *Phys. Rev.* B **19** 6094–118
Williams A R, Moruzzi V L, Gelatt C D Jr, Kübler J and Schwarz K 1982 *J. Appl. Phys.* **53** 2019–23
Williams A R, Zeller R, Moruzzi V L, Gelatt C D Jr and Kübler J 1981 *J. Appl. Phys.* **52** 2067–9
You M V and Heine V 1982 *J. Phys. F: Met. Phys.* **12** 177–94